UvA-DARE (Digital Academic Repository)

Using a genome-scale metabolic model of Enterococcus faecalis V583 to assess amino acid uptake and its impact on central metabolism

Veith, N.; Solheim, M.; van Grinsven, K.W.A.; Olivier, B.G.; Levering, J.; Grosseholz, R.; Hugenholtz, J.; Holo, H.; Nes, I.; Teusink, B.; Kummer, U.

Link to publication

Using a Genome-Scale Metabolic Model of *Enterococcus faecalis* V583 To Assess Amino Acid Uptake and Its Impact on Central Metabolism

Nadine Veith,[a] Margrete Solheim,[b] Koen W. A. van Grinsven,[c] Brett G. Olivier,[d] Jennifer Levering,[a]* Ruth Grosseholz,[a]
Jeroen Hugenholtz,[c] Helge Holo,[b] Ingolf Nes,[b] Bas Teusink,[d] Ursula Kummer[a]

Department of Modeling Biological Processes, Center for Organismal Studies/Bioquant, Heidelberg University, Heidelberg, Germany[a]; Department of Chemistry, Biotechnology and Food Science, Norwegian University of Life Sciences, Aas, Norway[b]; Molecular Microbial Physiology, Swammerdam Institute for Life Sciences, University of Amsterdam and Netherlands Institute of Systems Biology, Amsterdam, The Netherlands[c]; Systems Bioinformatics, Amsterdam Institute for Molecules, Medicines, and Systems, VU University of Amsterdam, Amsterdam, The Netherlands[d]

Increasing antibiotic resistance in pathogenic bacteria necessitates the development of new medication strategies. Interfering with the metabolic network of the pathogen can provide novel drug targets but simultaneously requires a deeper and more detailed organism-specific understanding of the metabolism, which is often surprisingly sparse. In light of this, we reconstructed a genome-scale metabolic model of the pathogen *Enterococcus faecalis* V583. The manually curated metabolic network comprises 642 metabolites and 706 reactions. We experimentally determined metabolic profiles of *E. faecalis* grown in chemically defined medium in an anaerobic chemostat setup at different dilution rates and calculated the net uptake and product fluxes to constrain the model. We computed growth-associated energy and maintenance parameters and studied flux distributions through the metabolic network. Amino acid auxotrophies were identified experimentally for model validation and revealed seven essential amino acids. In addition, the important metabolic hub of glutamine/glutamate was altered by constructing a glutamine synthetase knockout mutant. The metabolic profile showed a slight shift in the fermentation pattern toward ethanol production and increased uptake rates of multiple amino acids, especially L-glutamine and L-glutamate. The model was used to understand the altered flux distributions in the mutant and provided an explanation for the experimentally observed redirection of the metabolic flux. We further highlighted the importance of gene-regulatory effects on the redirection of the metabolic fluxes upon perturbation. The genome-scale metabolic model presented here includes gene-protein-reaction associations, allowing a further use for biotechnological applications, for studying essential genes, proteins, or reactions, and the search for novel drug targets.

*E*nterococcus faecalis plays an important role in both biotechnology and medicine ([1], [2]). Some strains are used in the dairy industry for food fermentation and flavor production. At the same time, other strains play an increasingly important role as pathogens, especially in hospital-acquired infections ([1]). *E. faecalis* strains show multiple antibiotic resistances and are therefore the cause of serious complications. Alternative strategies for combating multiple resistant bacteria such as *E. faecalis* are urgently needed. Targeting vulnerable points in the bacterial metabolism could offer such an alternative route and has been discussed as a promising strategy ([3], [4]). However, surprisingly little is known about the detailed metabolism of *E. faecalis*, and it is therefore mandatory to explore this in a more elaborate fashion than previously reported.

E. faecalis shows a high stress tolerance and is adapted to a variety of different native environments ranging from soil up to human or animal digestive tracts ([1], [2]). This environmental variability requires a highly flexible metabolic system to quickly adapt to diverse and changing environmental conditions. Therefore, strategies that target the bacterial metabolism must take this flexibility into account and must use a systemic view on the entire metabolism.

Computational models allow studying the properties and dynamics of complex metabolic networks and may allow the identification of potential new drug targets. Of the different approaches available, kinetic models allow a quantitative investigation of the dynamics of specific metabolic behavior and offer a very detailed and quantitative view on the involved mechanisms. However, they also require detailed knowledge of the involved reaction kinetics and the associated kinetic parameters. Genome-scale stoichiometric models, on the other hand, lack this detail and also only require the information about the stoichiometry of the individual reactions, which is more readily available ([5]). They can offer a complete overview of the stoichiometric network of the cell, allowing the identification of essential processes and the associated genes and enabling an at least semiquantitative view of how fluxes can be distributed in a complete metabolic network using constraint-based modeling techniques. Constraints are represented by physicochemical constraints such as mass or charge

balances and reaction reversibility. The environment and the physiology of the organism are reflected by input and export fluxes. On the basis of these constraints, genome-scale metabolic models are used to characterize the metabolic capabilities of an organism and are used for the prediction of growth rates, minimal media, or maximal metabolite production rates (6).

At present, genome-scale models of many organisms are available. Within the group of lactic acid bacteria, the genome-scale metabolic model of *Lactobacillus plantarum* provided novel insights into the amino acid catabolism (7). The model was used to define a minimal growth medium, determine energy parameters for growth and maintenance, and revealed the presence of futile cycles under rich growth conditions. A recently published genome-scale model of the lactic acid bacterium *Lactococcus lactis* focused in detail on flavor-forming pathways that might have important implications in dairy industry, where this organism is frequently used (8). Outside the group of lactic acid bacteria, it is worth mentioning the genome-scale model of the human pathogen *Listeria monocytogenes* that was studied in a novel combination with transcriptome data and revealed a strong link between changes in the metabolism and induction of virulence (9). Another interesting example is the genome-scale model of the pathogen *Mycobacterium tuberculosis*. Here, gene-protein-reaction associations were integrated and used to predict lethal gene mutations and potential drug targets (10, 11).

Following a similar strategy, we set up a genome-scale metabolic model of the vancomycin-resistant human pathogen *E. faecalis* V583 based on the genomic information comprising the overall cellular metabolism as required for growth. The model allowed us to learn about the metabolic capabilities of the organism and to study the network behavior at different experimental conditions. We used constraint-based modeling techniques, computed energy parameters for maintenance and growth-associated processes based on anaerobic glucose-limited chemostat conditions, and compared biomass formation at different growth rates. The model constraints were based on experimentally measured uptake and product fluxes. Amino acid auxotrophy experiments were performed for model validation. Since L-glutamate and L-glutamine play a central role in amino acid metabolism and the incorporation of free ammonium ions into metabolites with implications on many pathways, we constructed an L-glutamine synthetase mutant ($\Delta glnA$) of *E. faecalis* and compared it to the wild type. With the genome-scale model, we could link changes in the fermentation pattern to changes in the amino acid uptake profiles.

MATERIALS AND METHODS

Bacterial strains and growth conditions. The bacterial strains and plasmids used in the present study are listed in Table 1. *E. faecalis* V583 (12) was grown anaerobically at 37°C in the chemically defined medium for lactic acid bacteria (CDM-LAB) medium containing (per liter): 1 g of K_2HPO_4, 5 g of KH_2PO_4, 0.6 g of ammonium citrate, 1 g of sodium acetate, 2.5 g of $NaHCO_3$, 0.25 g of tyrosine, 0.24 g of alanine, 0.5 g of arginine, 0.42 g of aspartic acid, 0.13 g of cysteine, 0.5 g of glutamic acid, 0.15 g of histidine, 0.21 g of isoleucine, 0.475 g of leucine, 0.44 g of lysine, 0.275 g of phenylalanine, 0.675 g of proline, 0.34 g of serine, 0.225 g of threonine, 0.05 g of tryptophan, 0.325 g of valine, 0.175 g of glycine, 0.125 g of methionine, 0.1 g of asparagine, 0.2 g of glutamine (0.4 g of glutamine for the $\Delta glnA$ mutant), 11 g of glucose, 0.5 g of L-ascorbic acid, 38.5 mg of adenine sulfate, 27.5 mg of guanine, 22 mg of uracil, 50 mg of cysteine, 10 mg of xanthine, 2.5 mg of D-biotin, 1 mg of vitamin B_{12}, 1 mg of riboflavin, 5 mg of pyridoxamine-HCl, 10 μg of *p*-aminobenzoic acid, 1 mg of pan-

TABLE 1 Bacterial strains and plasmids

Strain or plasmid	Characteristics	Source or reference
Strains		
E. coli EC1000		59
E. faecalis		
V583	Parental strain (ATCC 700802)	12
$\Delta glnA$ mutant	*glnA* knockout mutant	This study
Plasmids		
pCR-Blunt II-TOPO		Life Technologies
pLT06	Integrational vector; P-*pheS* counterselectable marker	17

tothenate, 5 mg of inosine, 1 mg of nicotinic acid, 5 mg orotic acid, 2 mg of pyridoxine, 1 mg of thiamine, 2.5 mg of lipoic acid, 5 mg of thymidine, 200 mg of $MgCl_2$, 50 mg of $CaCl_2$, 16 mg of $MnCl_2$, 3 mg of $FeCl_3$, 5 mg of $FeCl_2$, 5 mg of $ZnSO_4$, 2.5 mg of $CoSO_4$, 2.5 mg of $CuSO_4$, and 2.5 mg of $(NH_4)_6Mo_7O_{24}$ (13).

Chemostat cultures were grown in a Biostat B plus fermentor (Sartorius Stedim Biotech) with a working volume of 750 ml at dilution rates (d) of 0.05, 0.15, and 0.4 h^{-1}. The bioreactor was set for both pH (pH 6.5) and temperature (37°C) control. For pH control, sterile 4 M NaOH was automatically added. Cultivation was carried out under anaerobic condition (60 ml/min N_2), with a stirring speed of 250 rpm. The cultures were considered to be in steady state when there was no detectable glucose in the culture supernatants and the optical density, cell dry weight, and product concentrations of the cultures were constant in samples taken on two consecutive days. Samples used for metabolite analysis were taken from cultures grown for six generations after the sample confirming steady state had been taken. All experiments were performed in triplicate.

Culture samples of 20 to 50 ml were centrifuged at 4°C at 6,000 × *g* for 10 min, and pellets were treated according to the protocols for measuring the dry weight as previously described (14). Supernatants were frozen at −20°C until metabolite analysis.

Metabolite measurement. After removal of bacterial cells by centrifugation (5 min, 6,000 × *g*), the metabolites were analyzed by high-performance liquid chromatography (HPLC) and headspace gas chromatography, as previously described (15). Amino acid analysis was performed using HPLC with a 1:1 (vol/vol) ratio of sample supernatant and internal standard solution (0.1 M HCl, 0.4 μmol of L-Norvalin/ml; Sigma) as previously described (16).

Generation of $\Delta glnA$ mutant. *E. faecalis* V583 and the vector pLT06 were used for generation of a *glnA* deletion mutant (17). The ∼800- and 500-bp regions upstream and downstream of the target gene were amplified using the primer pairs glnA-5 (AAAAAGTTCATAAATGGAACAC TCG) and glnA-6 (CGACATTATGGGAACAATTAAAAATTTGGAGTT GTACTAAAAGCCGTTAC) and glnA-7 (ATTTTTAATTGTTCCCATAAT GTCG) and glnA-8 (GTTTTTTCCAATTGGTACAGTTATGA), respectively. The PCR products were ligated and reamplified using the primers glnA-5 and glnA-8, resulting in a 1.3-kb product. The 1.3-kb PCR product was subcloned into pCR-Blunt-TOPO (Life Technologies) and then excised by BamHI and PstI and ligated with pLT06. The resulting construct was propagated in *Escherichia coli* EC1000 and grown on Luria broth (LB) agar plates containing 15 μg of chloramphenicol (Cm) and 20 μg of X-Gal (5-bromo-4-chloro-3-indolyl-β-D-galactopyranoside)/ml at 30°C. Blue colonies were screened for the presence of the 1.3-kb insert using the primers OriF and KS05SeqR (17). Positive clones were grown overnight in liquid LB medium containing Cm at 30°C. The plasmid was purified by using an ENZA plasmid minikit (Omega Bio-Tek), and the insert was sequenced to confirm the integrity. The deletion construct was then transformed into *E. faecalis* V583 by electroporation as described previously (18), and double-

crossover markerless deletion of *glnA* was obtained as previously described (17).

Reconstruction of the metabolic network. The first step in building a genome-scale model of *E. faecalis* was the reconstruction of the metabolic network from the genome sequence of *E. faecalis* V583. This process was accelerated by using the AUTOGRAPH (automatic transfer by orthology of gene reaction associations for pathway heuristics) method (19). The second step was the extensive gap filling and manual curation process of the predicted metabolic network based on the information in Uniprot, KEGG, and partially EnteroCyc (http://enterocyc.broadinstitute.org), as well as on literature information. For the function assignment of transport reactions, the TransportDB and TCDB (Transport Classification Database) databases were used. If no genes were found even though experimental evidence about a metabolic reaction exists, the reaction was included as a "non-gene-associated reaction." Gene-protein-reaction assignments were based on the reference genome-scale models of *L. plantarum*, *L. lactis*, *B. subtilis*, *E. coli*, and literature or database information. A detailed description of the reconstruction and the model building process was published previously (20).

Model construction. The reconstructed metabolic network was used to build the genome-scale metabolic model by using the software PySCeS CBMPy, a python-based framework for stoichiometric modeling (http://cbmpy.sourceforge.net) (21). We used an implemented task in PySCeS CBMPy to guarantee mass and charge balance. We further tested the genome-scale model for the presence of loops, as reported for the genome-scale model of *L. lactis* (8). The model was annotated and exported as SBML level 3 (22) and will be publicly available in BIOMODLES and SysMO SEEK and is additionally provided as a spread sheet in the appendix (see Table SA1 in the supplemental material). The model reactions are described by reaction names and EC numbers. The metabolites are characterized by elemental formula, charge state, and ChEBI identifiers (23).

Model simulation. Experimental constraints are represented as uptake and product fluxes based on experimentally measured metabolite concentrations. The fluxes q_i are calculated as shown in an equation: $q_i = ([C_{supernatant}] - [C_{medium}]) \cdot d/X$, where C represents the concentration of a measured metabolite in mmol liter^{-1}, d is the dilution rate in h^{-1}, and X is the dry weight of cells in grams (gDW) liter^{-1}. For other medium components, theoretical uptake rates (q_{itheor}) were calculated by setting $C_{supernatant}$ to zero.

The experimental constraints were then defined as flux bounds for the respective exchange reactions in the model. Upper and lower bounds (u and l, respectively) were defined as $q_i \pm |SD|$ (the absolute value of the standard deviation), but at least $q_i \pm 10\%$. Thus, $S \cdot v = 0$, $l_j \leq q_i \leq u_j$ for all measured fluxes q_i, $l_i \leq q_{itheor} \leq u_i$, and $\mu = d$, where S represents the stoichiometric matrix, v the flux vector, and μ the growth rate.

In the case of L-glutamine, the HPLC analysis resulted in a constant underestimation of the medium concentration compared to the theoretically used L-glutamine concentration. We therefore corrected the lower bound of the L-glutamine uptake flux for the observed divergence. All measured metabolite fluxes, including the flux bounds, are presented in the supplemental material (see Table SA2).

We defined maximal growth as an objective function and applied flux balance analysis (FBA) to compute optimal flux distributions through the metabolic system. Since we used specific uptake rates as constraints, the flux through the biomass equation corresponds to the specific growth rate (mmol gDW^{-1} h^{-1}) and effectively FBA finds the optimal yield strategies (24, 25) since the maximal growth rate is conditional on the input fluxes.

We further used flux variability analysis (FVA) (26) in order to study feasible flux ranges. Both FBA and FVA were applied as implemented in PySCeS CBMPy, including IBM ILOG CPLEX, to solve the optimization problems.

Computation of growth-associated and non-growth-associated energy parameters. A detailed description of the computation of energy parameters with a genome-scale metabolic model was reported by Teusink et al. (7). For the traditional method, the energy parameters were estimated from the experimentally measured fluxes of fermentation products by summing up the fluxes of L-lactate, ethanol, and 1.5 times the flux of acetate. In order to directly compare the traditional and the computational method, the reduced cost value of the biomass flux on the maximal ATP production rate was calculated and combined with the previously computed energy parameter for biomass assembly.

Analysis of the flux distribution between mixed acid and homolactic fermentation. We used FVA to study the flux distribution between mixed acid (production of ethanol, acetate, and *R*-acetoin) and homolactic (production of L-lactate) fermentation. Since the amount of *R*-acetoin is comparatively small, we did not consider this metabolite in the subsequent analysis. First, we computed the possible flux ranges while applying the experimentally determined uptake and product fluxes as flux bounds on the exchange reactions. Second, we computed an FVA again, for which we released the flux bounds on the fermentation products L-lactate, ethanol, and acetate while setting the lower and upper flux bounds to 0 and 1,000, respectively. To maintain comparability, we kept the specific growth rate constant. The increased ATP consumption rate was translated into the model by increasing the lower bound of the ATP maintenance reaction (by 7 mmol gDW^{-1} h^{-1}). An increased NAD$^+$ requirement (by 7 mmol gDW^{-1} h^{-1}) was introduced by an artificial NAD$^+$-consuming reaction that resulted in NADH production.

Simulation of amino acid auxotrophies. The omission of an amino acid in the growth medium was simulated by changing the respective exchange flux in the model to zero. If FBA resulted in an optimal solution, the respective amino acid was predicted to be nonessential. In cases where no feasible solution was observed, the respective amino acid was predicted to be essential. To be able to compute realistic results and prevent false-negative predictions, we relaxed the constraints on the exchange reactions such that upper and lower bounds of the amino acid exchange reactions were set to "−1, 0" or "0, 1". The direction of the amino acid exchange fluxes were kept constant.

RESULTS

Reconstruction of the genome-scale metabolic model. We generated a genome-scale model of the central metabolism of *E. faecalis* V583 based on its genome sequence (28). The model contains all metabolic reactions that are required for cell growth in CDM-LAB medium (13): the central energy metabolism (glycolysis, fermentation, pentose phosphate pathway), the nucleotide biosynthesis and the production of DNA and RNA, the amino acid metabolism and protein biosynthesis, the synthesis of vitamins and cofactors, the fatty acid biosynthesis, the production of phospholipids and its derivatives, and teichoic acid production, as well as the biosynthesis of peptidoglycan and capsular polysaccharides. All reactions are listed in Table SA1 in the supplemental material.

An initial draft of the metabolic network was automatically reconstructed by the AUTOGRAPH method (19). This method uses orthology searches against existing genome-scale models to predict genes in a genome sequence that code for metabolic reactions and their respective metabolic function. Identification of "metabolic" genes and the respective function predictions were based on the existing, well-curated genome-scale models of *L. plantarum*, *L. lactis*, *Bacillus subtilis*, and *Escherichia coli* (7, 29–31). A genome-scale model of *L. plantarum* served as the template model for setting up the individual reaction equations of each metabolic reaction that are common in both lactic acid bacteria. The initial draft was then manually refined by adding metabolic reactions that are specific for *E. faecalis* based on the genome sequence and/or literature information.

Further extensive manual curation was necessary since many metabolic pathways were incomplete or contained gaps where one or more genes were either missing or are not yet annotated. We

TABLE 2 Characteristics of genome-scale metabolic model of *E. faecalis* V583

Gene, reaction, or metabolite	Total no. (%)
Genes	
In genome[a]	3,412
In model	668 (19.6)
Reactions	706
Non-gene associated[b]	183
Blocked	152
Balanced	553
Exchange	72
Transport	128
Metabolites	642
Extracellular	105
Intracellular	537

[a] Chromosome and plasmids (NCBI webserver, genome database).
[b] Inclusive exchange reactions and reactions representing the assembly of macromolecules.

performed extensive literature studies to find information about the presence or absence of both genes and gene functions, and we applied homology searches to identify genes and gene functions that are not yet annotated in the *E. faecalis* V583 genome.

In the end, the newly constructed genome-scale model contained 642 metabolites and 706 reactions in total. A summary of the model features is shown in Table 2. The model consists of metabolic reactions within the cell and the transport reactions that represent the uptake of nutrients and the export of metabolic end products by the cell, as well as exchange reactions that describe the exchange of metabolites with the environment.

Constraint-based modeling. The finalized genome-scale model provided insights into the metabolic capabilities and adaptations of *E. faecalis* by allowing us to study the flux distribution through the metabolic network. We defined additional constraints to restrict the model behavior to physicochemically and biologically feasible states only. We ensured mass and charge balance and defined irreversible reaction steps for enzymatic reactions, which are reported to be "irreversible" on a macroscopic scale. Information about reaction reversibility were based on the template model of *L. plantarum* or derived by literature search. We identified physiologically relevant flux distributions through the metabolic network by using flux balance analysis (FBA) (32–34). For this purpose, a biologically meaningful objective function had to be defined. Since maximal growth seems to be a reasonable objective for microbes, we defined the flux through the biomass equation to be maximized as objective function (32, 33). The biomass equation is a phenomenological description of the cell composition. It sums up all macromolecules that build a cell. The corresponding stoichiometric information was derived from the genome-scale model of *L. plantarum* (7) since, to our knowledge, no information is available about the exact biomass composition of *E. faecalis*.

Since FBA does often not result in one unique flux distribution and alternative optimal flux distributions exist that satisfy the same constraints, we also applied flux variability analysis (FVA) (26). FVA calculates a range (or interval) of possible flux values for each flux in the model while satisfying the constraints and reaching the same optimal value.

In addition, we applied constraints in the form of uptake and production fluxes based on experimental data to learn about physiological flux distributions. For this purpose, *E. faecalis* V583 was cultured in a glucose-limited anaerobic chemostat at three different dilution rates: 0.05, 0.15, and 0.4 h^{-1}. The metabolite concentrations of glucose, the fermentation end products and amino acids in the medium, and the supernatant of the cultures were measured (Fig. 1) and used to compute the net uptake or production fluxes (see Materials and Methods).

Under steady-state conditions, the dilution rate equals the growth rate of the cells. By constraining the model with the net uptake or product fluxes, represented as exchange fluxes in the model, we were able to predict the growth rate by maximizing the flux through the biomass function and compare the network behavior at different growth rates.

Energy parameters of *E. faecalis* V583. The ATP demand is one of the central aspects in microbial metabolism since ATP is required for cell growth and maintenance. Traditionally, the energy requirement for growth-associated processes (sa$_{ATP}$) and maintenance (m$_{ATP}$) were calculated from experimentally measured fluxes of the fermentation products L-lactate, acetate, and ethanol at different dilution rates. The fermentation fluxes were used to calculate the total ATP production rates at the respective dilution rates (35). However, the traditional method relies only on fermentation product formation for estimating energy parameters and does not account for additional metabolic substrates such as L-ascorbate or various amino acids that can contribute to the energy production without products feeding into fermentation.

The computation of energy parameters for growth and maintenance is a central aspect in genome-scale metabolic models (36). The model distinguishes between growth-associated energies required for macromolecule biosynthesis (s$_{ATP}$) and the assembly macromolecules in the biomass equation (a$_{ATP}$). The sum of both is estimated by the traditional method, whereas only the parameter for the latter one is required for the genome-scale metabolic model because the amount of energy that is required to form macromolecules is already accounted for by the stoichiometric network.

With the genome-scale metabolic model, we obtained a maintenance coefficient (m$_{ATP}$) of 0.81 mmol h^{-1} gDW^{-1} and an ATP demand for the assembly of macromolecules (a$_{ATP}$) of 26.48 mmol gDW^{-1}. The estimated coefficients are similar to the values as previously reported for the genome-scale models of *L. plantarum* and *L. lactis* (7, 8).

In order to compare the results observed with the genome-scale metabolic model with the traditional method, the amount of energy that is required for macromolecule biosynthesis (s$_{ATP}$) must be computed. This parameter is equal to the relative effect of the flux through the biomass equation on the maximal ATP production rate. When summing up the computed energy parameters for macromolecule biosynthesis and assembly, similar results were observed for the computational (sa$_{ATP}$ = 69.3 mmol gDW^{-1}; m$_{ATP}$ = 0.6 mmol h^{-1} gDW^{-1}) and traditional (sa$_{ATP}$ = 71.2 mmol gDW^{-1}; m$_{ATP}$ = 0.7 mmol h^{-1} gDW^{-1}) methods.

Fermentation pattern of *E. faecalis* V583. In *E. faecalis*, the fermentation pattern is affected by the growth rate (37). In our experiments, a transition from mixed acid fermentation to increased homolactic fermentation was observed while changing the dilution rate from low to intermediate and high dilution rates (Fig. 1). Mixed acid fermentation results in a higher yield of ATP
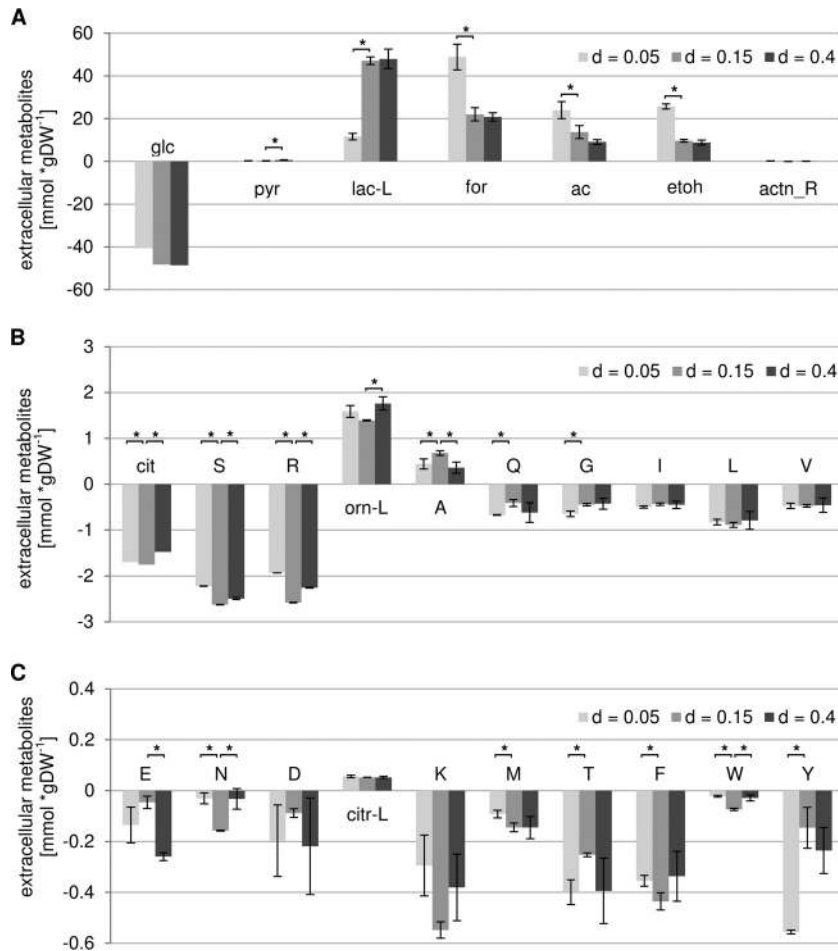
FIG 1 Experimentally measured metabolites consumed and produced by *E. faecalis* V583. (A) Consumption of glucose and production of fermentation products at three different dilution rates (*d*). (B and C) Results for citrate, amino acids, and some derivatives. Consumed metabolites are represented by negative values, and produced ones are represented by positive values. All metabolite concentrations were averaged over three data sets, and the standard deviations are displayed, except for the amino acid concentrations measured at a dilution rate of 0.15 h^{-1}, which were averaged over two datasets. Significant differences in the metabolite data were computed with Student's *t* test and indicated for *P* values of <0.05. glc, glucose; cit, citrate; pyr, pyruvate; lac-L, L-lactate; for, formate; ac, acetate; etoh, ethanol; actn_R, R-acetoin; orn-L, L-ornithine; citr-L, L-citrulline. The amino acids are represented in one-letter code style.

than homolactic fermentation. The mechanism that causes a switch from homolactic to mixed acid fermentation or vice versa is not yet fully understood, but it involves the growth rate-dependent regulation of pyruvate formate lyase (EC 2.3.1.54) expression. In addition to the growth rate (37) and the glucose concentration, the culture pH seems to play a role as reported by Fiedler et al. (13), who observed a shift to more homolactic fermentation at a low culture pH.

We used FVA and analyzed the flux distribution between the reactions of the mixed acid and homolactic fermentation. The experimentally determined net uptake and production fluxes (Fig. 1) were applied as experimental constraints in the form of flux bounds that restrict the uptake and product fluxes in the model (Fig. 2A, thick black lines). Next, we released the experimentally observed flux bounds for the fermentation products L-lactate, acetate, ethanol, and formate (Fig. 2A, gray bars). While comparing the ranges of the possible fermentation product fluxes in the model, no preference for homolactic or mixed acid fermentation could be observed. Based on the model and the experimental constraints, we suggest that there are not stoichiometric but rather
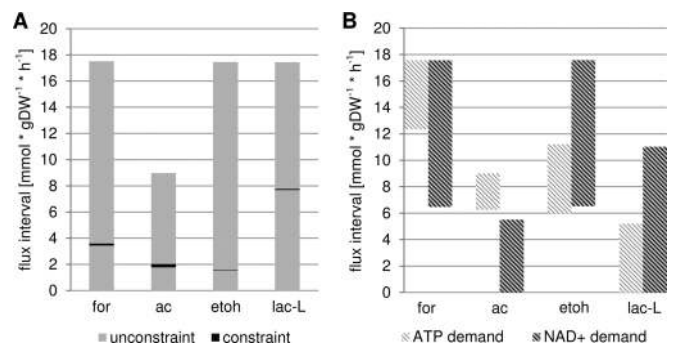
FIG 2 Comparison of constraint and unconstraint feasible flux ranges for the fermentation product fluxes. (A) Feasible flux ranges for a dilution rate of 0.15 h^{-1} when all experimentally determined metabolite fluxes are applied as constraints (black section) and flux ranges when the constraints of the fermentation product fluxes are released (gray section). (B) Changes in the flux intervals when an additional artificial ATP (light gray bars) or NAD$^+$ (dark gray bars) requirement is introduced. for, formate; ac, acetate; etoh, ethanol; lac-L, L-lactate;.

regulatory effects that are crucial for the decision between mixed acid and homolactic fermentation, at least under these conditions. Although the regulatory mechanism remains unclear, both an increased ATP demand and an increased NADH/NAD$^+$ ratio showed the potential to redirect the model flux toward mixed acid fermentation (Fig. 2B) based on the experimental constraints used here.

Amino acid auxotrophies. The amino acid metabolism of *E. faecalis* V583 is not fully characterized. Many enzymes are not annotated, and there seem to be many strain-specific differences. Murray et al. studied the amino acid auxotrophies of 23 different *E. faecalis* strains (38). According to the results of Murray et al., these strains share common auxotrophies of only four amino acids, i.e., L-histidine, L-isoleucine, L-methionine, and L-tryptophan, whereas high variability is observed for most other amino acids. This high strain specificity might be related to adaptation to the various different native environments of different *E. faecalis* strains. Since the studies of Murray et al. did not include the vancomycin-resistant strain V583, we experimentally performed amino acid "leave-out" experiments to understand completely the essentiality of amino acids in *E. faecalis* V583 and concomitantly to validate our genome-scale model. Therefore, *E. faecalis* V583 was inoculated in batch cultures in CDM-LAB medium where one or two amino acids were omitted from the medium and cell growth was monitored. To account for adaptation processes such as changes in gene expression, we performed sequential inoculation steps, where the cells were cultured for 24 h in the respective medium, washed, and transferred to fresh medium again. This method allowed the removal of residual amounts of the respective amino acid from the growth medium and thus allowed us to better distinguish between prototrophy and auxotrophy (Fig. 3A). The amino acids L-histidine, L-arginine, and L-tryptophan, the branched-chain amino acids, and L-methionine were observed to be essential. We further defined a threshold (optical density at 600 nm of <0.3) to distinguish between growing and nongrowing cultures to reduce false-positive predictions. The threshold was defined such that all confirmed essential amino acids (based on literature information or the fact that all genes required for biosynthesis are absent) fall directly below the threshold. With this strategy, the interpretation for glycine was ambiguous, since the visually observed growth only marginally passed the threshold during the first two subsequent inoculations. After the third inoculation, the final optical density obtained was well above the threshold, suggesting that glycine might be considered nonessential (Fig. 3C). However, as discussed below, alternative explanations with glycine being essential are also still possible.

We used the experimental information of the amino acid auxotrophies to validate the reconstructed metabolic network. We have reconstructed the amino acid metabolism based on initial annotations and subsequent intense manual curation using homology searches and literature. One difficulty in the reconstruction is that some enzymes in the amino acid metabolism are characterized by a weak substrate or reaction specificity, which makes a precise network prediction difficult. Thus, we estimated both the specific substrate specificity and the reaction reversibility based on information from closely related organisms. In cases of the degradation of sulfur compounds, such as methionine, weak substrate and reaction specificity was observed (39, 40). The presence of certain degradation routes can only be inferred from measurements of volatile sulfur compounds (41). For the validation of the

metabolic network, we simulated the amino acid auxotrophy experiments and could successfully predict all amino acid auxotrophies with the genome-scale metabolic model (Fig. 3D).

We also performed double leave-out experiments for some amino acids where we simultaneously omitted two amino acids in the culture medium. Since we observed very weak growth when glycine was omitted, we performed a double-leave-out experiment wherein glycine and L-serine were absent in the culture medium (Fig. 3A and C). Since *E. faecalis* seems to lack threonine aldolase (EC 4.1.2.5), glycine appears to be only producible from L-serine by glycine hydroxymethyltransferase (GHMT) (*glyA*; EF2250; EC 4.4.1.1). GHMT catalyzes the reversible conversion of L-serine into glycine while producing 5,10-methylene tetrahydrofolate from tetrahydrofolate, respectively. Tetrahydrofolate derivatives, such as 5,10-methylene tetrahydrofolate, form the C$_1$ folate pool, an important pool of metabolites that supply CH$_3$-moieties for many metabolic pathways like the nucleotide biosynthesis (42). Upon omitting both glycine and L-serine from the culture medium, we experimentally detected weak growth, whereas normal growth was detected *in silico*. One possible explanation for this observation, namely, poor growth in the absence of glycine alone and in the absence of both glycine and L-serine, might be a regulatory effect on the transcriptome level. In *L. lactis*, the gene *glyA* that codes for GHMT, as well as several genes of the C$_1$ folate metabolism, is reported to be under the control of PurR, a transcriptional regulator of purine biosynthesis (43). PurR activity was shown to be affected by the presence of the purine hypoxanthine and PRPP. Assuming that the transcription of the GHMT gene is low or absent under our experimental conditions, the omission of glycine will not be sensed by the cell directly, and growth will be significantly reduced as long as sufficient nucleotides are available. A PurR repressor protein was identified on the genome of *E. faecalis* V583 (*purR*, EF0058) sharing high sequence identity with the one of *B. subtilis* (0.55 sequence identity) and *L. lactis* MG1363 (0.53 sequence identity) (see Table SA1 in the supplemental material). A PurR binding motif that resembles the consensus sequence of *L. lactis* and *B. subtilis* was found upstream of the *glyA* gene in *E. faecalis*, which suggests the presence of a similar PurR based regulatory mechanism in this organism (see Table SA2 in the supplemental material).

We also performed double-leave-out experiments for amino acids that are involved in central nitrogen metabolism, namely, L-aspartate and L-asparagine, as well as L-glutamic acid and L-glutamine (Fig. 3B). The combined omission of L-asparagine and L-aspartate did not lead to growth inhibition, whereas the simultaneous omission of L-glutamine and L-glutamate did lead to growth inhibition. The model predictions were in agreement with the experimental findings. The metabolic network shows that L-glutamate and L-glutamine can be converted into L-aspartate and L-asparagine but not vice versa. In the model, L-aspartate, and subsequently L-asparagine, can be produced by the aspartate transaminase (ASPTA; EC 2.6.1.1), which catalyzes the reversible transamination of oxaloacetate to L-aspartate while converting L-glutamate to 2-oxoglutarate. The latter metabolite can be recycled to L-glutamate by the glutamate dehydrogenase (GDH; EC 1.4.1.4) reaction (Fig. 4). Since L-glutamate and 2-oxoglutarate form a balanced pool in *E. faecalis*, L-glutamate formation from L-aspartate by the reverse reaction of ASPTA is not possible under steady-state conditions. Furthermore, there is no indication for an L-glutamate *de novo* biosynthetic pathway in *E. faecalis*. This ex-
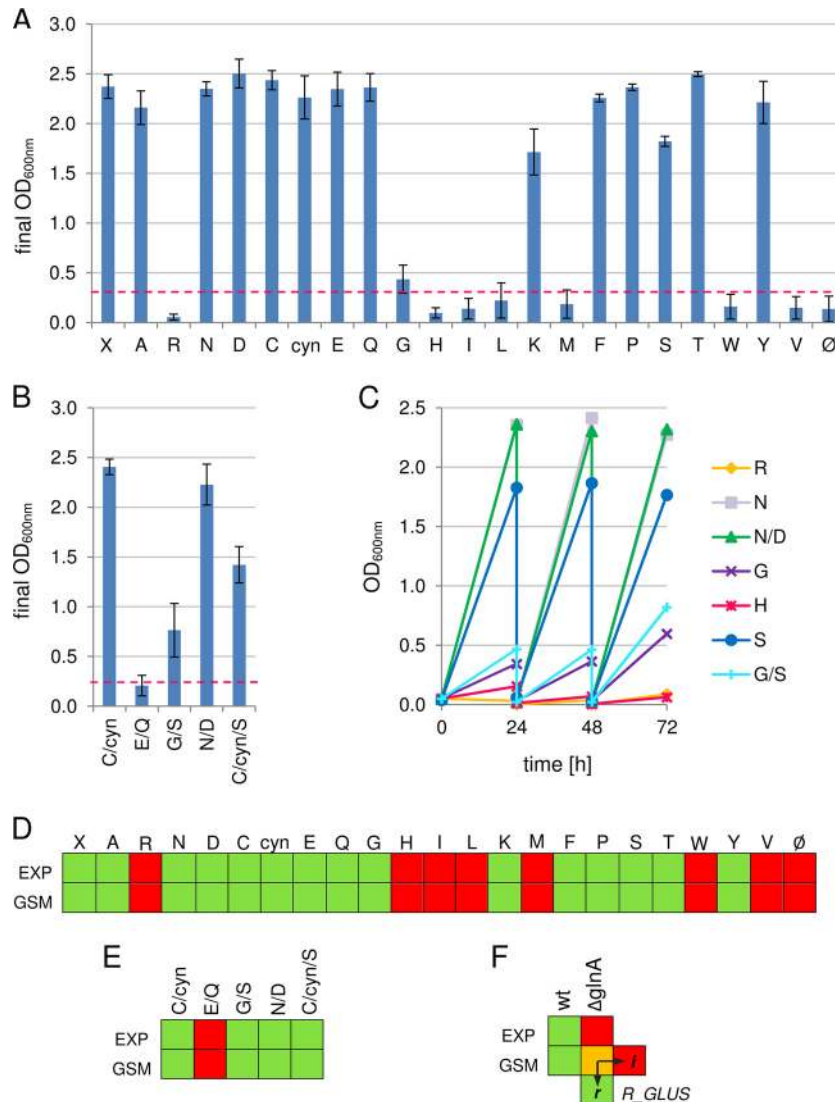
FIG 3 Amino acid auxotrophy experiments with *E. faecalis* V583. (A) Averaged final optical density (OD) during three consecutive passages over 72 h while omitting single amino acids from the growth medium. We defined a threshold (OD > 0.3), indicated by the dashed red line, to distinguish growth from nongrowth. The standard deviation was calculated from OD measurements of three sequential inoculation steps. (B) Averaged final OD over 72 h while omitting simultaneously two or three amino acids. (C) Measured ODs at 24, 48, and 72 h. Cells were washed and reinoculated in fresh medium after every 24 h. (D and E) Comparison between the experimental results of the amino acid auxotrophy experiments (EXP) and the simulation results with the genome-scale metabolic model (GSM). Green squares indicate growth in the absence of the respective amino acid. Red represents no growth. (F) Comparison between EXP and GSM when omitting L-glutamine in either the wild-type (wt) culture or a glutamine synthase knockout mutant (ΔglnA) of *E. faecalis* V583. The yellow square indicates the dependence of the simulation results on the reversibility of the glutamate synthase reaction (R_GLUS). X, full growth medium; ø, no amino acids; cyn, L-cystine.

plains the growth impairment upon the simultaneous omission of L-glutamine and L-glutamate.

Glutamine synthetase mutant. To learn more about the central amino acid metabolism, we experimentally generated a glutamine synthase knockout mutant (Δ*glnA*) in *E. faecalis* V583. Glutamine synthetase (GLNA; *glnA*; EF2159; EC 1.4.1.13) catalyzes the ATP-dependent formation of L-glutamine from L-glutamate and NH_4^+ and therefore performs nitrogen assimilation for growth. In many lactic acid bacteria, *glnA* expression is highly upregulated and essential during growth in milk, whereas L-glutamine is present in trace amounts only (42, 44). In *E. faecalis*, the Δ*glnA* mutant was experimentally shown to be an auxotroph for

L-glutamine (Fig. 3F). In contrast, L-glutamine production was observed in the genome-scale metabolic model via the reverse reaction of the glutamate synthase (GLUS; EC 1.4.1.13). GLUS catalyzes the formation of two L-glutamate molecules from one molecule of L-glutamine and 2-oxoglutarate, respectively. Omitting the reverse reaction, the production of L-glutamine from L-glutamate in the genome-scale metabolic model abolishes *in silico* growth without L-glutamine. There is some evidence that the glutamate synthase of *Escherichia coli*, *Bacillus megaterium*, and *Bacillus licheniformis* are irreversible. These enzymes are reported to require the presence of L-glutamine and NADPH for activity (45–47). Assuming that there might be a similar sensitivity of the glu-
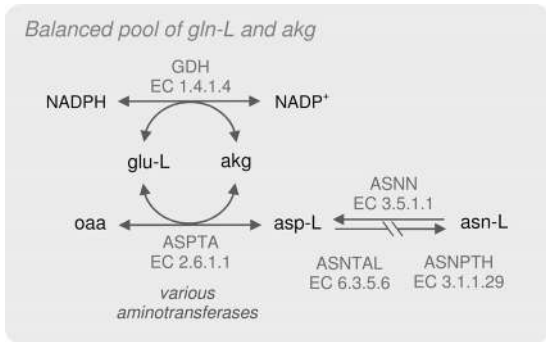
FIG 4 Schemata for L-glutamate and 2-oxoglutarate interconversion. L-Glutamate (glu-L) and 2-oxoglutarate (akg) form a balanced pool, though this is not the case for L-aspartate (asp-L) and L-asparagine (asn-L). Interrupted arrows indicate lumping of reactions. oaa, oxaloacetate; ASPTA, aspartate transaminase; GDH, glutamate dehydrogenase; ASNN, asparaginase; ASNTAL, asparaginyl-tRNA synthase (glutamine hydrolyzing); ASNPTH, aminoacyl-tRNA hydrolase.

tamate synthetase in *E. faecalis*, we defined the glutamate synthase reaction as an irreversible reaction. In addition to this, the glutamate synthase activities in *E. coli* and *B. subtilis* have both been shown to be inhibited by L-glutamate (47, 48). High intracellular concentrations of L-glutamate can therefore lead to a general inhibition of the glutamate synthase activity. In addition to the potential kinetic effects, which are obviously lacking in a stoichiometric model, the lack of expression of glutamate synthase at the experimental conditions used here could also explain the observed discrepancy. Omitting either the reverse reaction of GLUS or the complete reaction by a knockout of this reaction resulted in identical simulation results in the genome-scale metabolic model under the conditions applied here.

We further studied the metabolic profile of the ΔglnA mutant and used the metabolic genome-scale model to compare the behavior of the mutant to the wild-type strain of *E. faecalis* V583. The ΔglnA mutant shows a slight shift in the fermentation pattern away from L-lactate production toward increased ethanol production, accompanied by an increased formate production (Fig. 5).
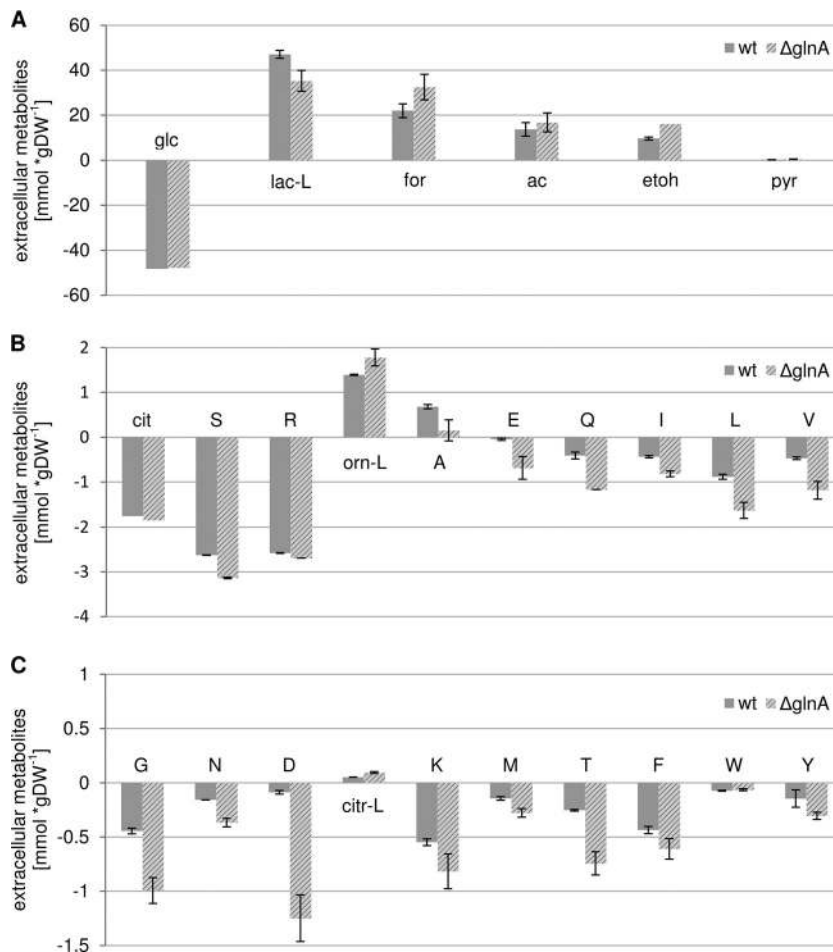

FIG 5 Experimentally measured metabolites consumed and produced by wild-type cultures and a glutamine synthetase mutant of *E. faecalis* V583. (A) Consumption of glucose and production of fermentation products at a dilution rate of 0.15 h^{-1}. (B and C) Similarly, results for citrate, amino acids, and some derivatives are shown. Consumed metabolites are represented by negative values, and produced ones are represented by positive values. All metabolite concentrations were averaged over three data sets, and the standard deviations are displayed, except for the amino acid concentrations of the wild-type data set, which were averaged over two datasets. Statistically significant changes computed with Student's *t* test and with a *P* value of <0.05 were observed for all metabolites except for L-tryptophan (W) and L-lysine (K). glc, glucose; cit, citrate; pyr, pyruvate; lac-L, L-lactate; for, formate; ac, acetate; etoh, ethanol; actn_R, R-acetoin; orn-L, L-ornithine; citr-L, L-citrulline. Amino acids are represented in one-letter code style.

Both ethanol and lactate production regenerate NAD^+, whereby ethanol fermentation results in the production of one additional NAD^+ compared to lactate production. Apart from this, the $\Delta glnA$ mutant shows also strongly altered amino acid profiles. The uptake rates of the many amino acids are increased, especially that of L-glutamine, but also those of L-glutamate, L-asparagine, and L-aspartate (Fig. 5). While studying the flux distributions through the genome-scale model, we were able to relate the shift from homolactic fermentation to increased ethanol production to the altered amino acid uptake profile in the following way.

In wild-type cells, different strategies are used to compensate the absence or low levels of L-glutamine intracellularly. One possibility is to upregulate L-glutamine uptake, which assumes L-glutamine is present in the growth medium. Another possibility is to increase the biosynthesis of L-glutamine and the uptake of its precursor, L-glutamate. In the $\Delta glnA$ mutant, both increased L-glutamine and L-glutamate uptake rates are observed compared to the uptake rates in wild-type cells (Fig. 5). The strongly increased uptake rates of both amino acids indicate the presence of a regulatory mechanism at the level of glutamine synthase.

In *L. lactis*, glutamine synthase and the glutamine uptake system are controlled by the transcription regulator GlnR (49), a repressor protein also found in *E. faecalis* V583 (EF2160). GlnR is known to repress enzymes of the nitrogen metabolism in the presence of L-glutamine (49, 50). In the $\Delta glnA$ mutant, the drop in the L-glutamine level might induce an increased transcription of L-glutamine and L-glutamate uptake systems, which results in the observed increased uptake rates.

The L-glutamine permease of *E. faecalis* was experimentally observed to have weak substrate specificities and is able to transport many other amino acids, such as L-asparagine with similar transport efficiencies (51). Upregulation of the L-glutamine permease may therefore account for the increased uptake rates of L-arginine, L-valine, L-threonine, L-tryptophan, glycine, L-methionine, L-cysteine, L-serine, and L-alanine. L-Glutamate and L-aspartate share a transport system in *E. faecalis*. An upregulation of the L-glutamate transport therefore readily explains the increase in the L-aspartic acid uptake rate (52).

In this model, the experimentally observed increased uptake rates of L-glutamine and L-glutamate in the *glnA* mutant require an additional degradation of both amino acids. Since there is no indication of an L-glutamine or an L-glutamate degradative pathway *in E. faecalis*, the model suggested the conversion of both amino acids into L-proline or folate and their derivatives (Fig. 6). The production of L-proline and folate from L-glutamate requires additional ATP, which is provided by the complete uptake and degradation of L-serine and the additional degradation of the branched-chain amino acids in the genome-scale metabolic model. This can explain the experimentally observed increased uptake rates of the branched-chain amino acids that could not be explained thus far (Fig. 5). The branched-chain amino acids are thought to be oxidized via the alpha-keto acid dehydrogenase complex (*bkdABCD*; EF1660, EF1659, EF1658, and EF1661) (53, 54). Thereby, one ATP is formed per branched-chain amino acid and NAD^+ is converted to NADH, which in turn requires additional regeneration of NAD^+ (53). Variations in the NADH/NAD^+ ratio can be sensed by transcription regulators of the Rex family (55), which might cause the system to change slightly from homolactic fermentation to ethanol production, as observed experimentally.

DISCUSSION

We constructed a new manually curated genome-scale metabolic model of *E. faecalis* V583 and studied physiological flux distributions within the metabolic network based on experimentally measured metabolic profiles of *E. faecalis* determined at different dilution rates. The metabolic data were used to constrain the genome-scale metabolic model and allowed us to compute energy parameters for growth-associated processes and maintenance. The metabolic network was validated against experimentally determined amino acid auxotrophies of the respective strains. The seven amino acids—L-arginine, L-histidine, L-methionine, L-tryptophan, and the branched-chain amino acids L-isoleucine, L-leucine, and L-valine—were found to be essential, as well as the combination of L-glutamate and L-glutamine. Growth in the absence of glycine was difficult to assess. To distinguish between growing and nongrowing cultures, we defined a threshold marginally higher than the optical density observed for cultures lacking proven essential amino acids. Depending on the selected threshold value, glycine could be assessed as an essential or a nonessential amino acid. Inherent point mutations, the absence of *glyA* gene expression, or the absence of glycine formation by GHMT are possible explanations for glycine auxotrophy. In order to assess the impact of this result, we took both possible scenarios into account when performing our model analyses. Neither an implemented glycine auxotrophy nor prototrophy affected presented modeling results discussed above.

To further study the amino acid metabolism, we constructed a $\Delta glnA$ mutant and compared its metabolic characteristics to those of the wild-type strain. We were able to predict the metabolic differences and related the experimentally observed changes in the flux distribution to potential gene regulatory mechanisms using the genome-scale model, thereby demonstrating that genome-scale metabolic models are useful tools to investigate the metabolic capabilities and possible flux distributions in a metabolic network.

We also studied the fermentation pattern at different growth rates where we introduced an artificial ATP and NAD^+ demand that both showed the potential to redirect the metabolic flux toward mixed acid fermentation. The role of NADH as an allosteric effector in regulation of gene expression through a transcriptional regulator of the Rex family was recently demonstrated in *E. faecalis* (55). Rex factors have been shown to sense the redox potential of the cell through changes in the NADH/NAD^+ balance, and genes that were demonstrated to be under the control of a Rex-like regulator in *E. faecalis* included *ldh* (EF0255, lactate dehydrogenase 1), *adhE* (EF0900, alcohol dehydrogenase), and *pflAB* (EF1612, pyruvate formate lyase-activating enzyme; EF1613, pyruvate formate lyase), among others (55).

Since transcriptional activation by transcription regulators of the Rex family activates enzymes of both mixed acid and homolactic fermentation, these regulators might not be the sole mechanism causing a switch in *E. faecalis*. When the enzymes of both pathways are expressed simultaneously, kinetic regulation of the enzyme activity might be responsible. In *L. lactis*, Garrigues et al. reported the accumulation of triose phosphates (glyceraldehyde 3-phosphate and dihydroxyacetone-phosphate) at high glycolytic flux that led to a subsequent inhibition of the pyruvate formate lyase (PFL; EC 2.3.1.54) and consequently to a redirection of the glycolytic flux toward L-lactate production (56). The accumula-
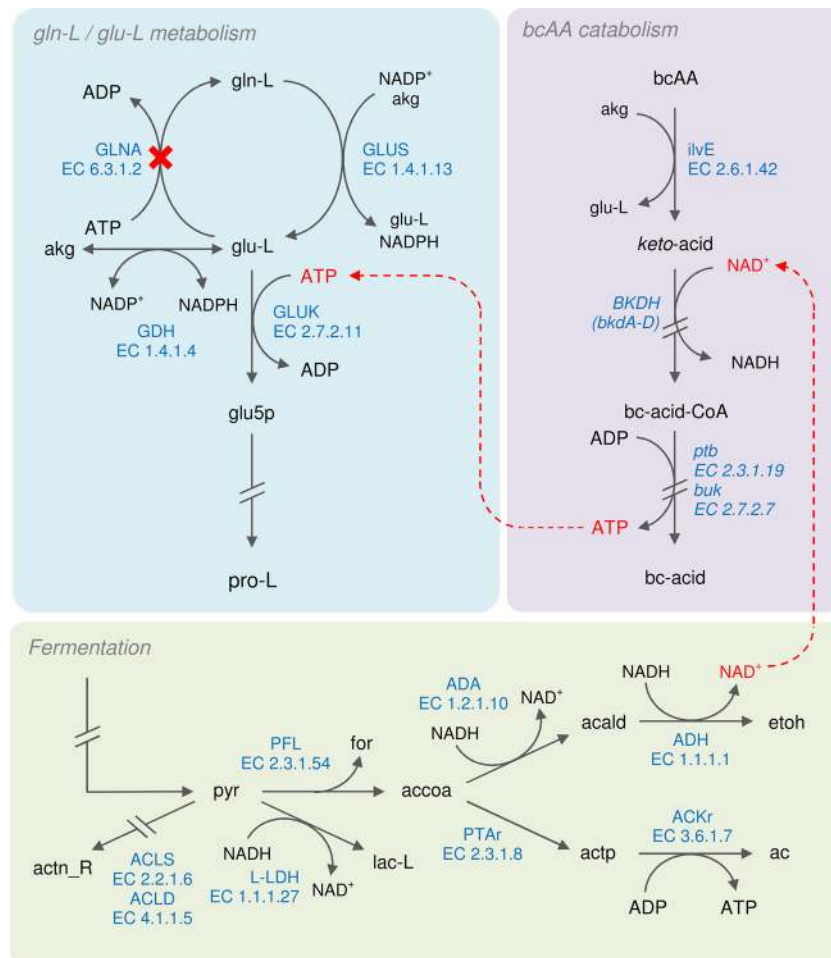
FIG 6 Coupling of metabolic pathways that lead to the redirection of the metabolic flux and the change in the fermentation pattern in the glutamine synthetase mutant of *E. faecalis* V583. The metabolic scheme shows three metabolic pathways: the L-glutamine and L-glutamate (gln-L/glu-L) metabolism, the branched-chain amino acid (bcAA) metabolism, and the fermentation. Dashed lines show exemplarily the coupling between the three pathways. Interrupted arrows indicate lumping of reactions. The enzymes responsible for single reaction steps are indicated in blue with its respective enzyme commission number (EC number). The knockdown of the glutamine synthetase reaction (GLNA) is indicated by a red "×." The production or consumption of protons and phosphate ions is not displayed. glu5p, L-glutamine-5-phosphate; accoa, acetyl coenzyme A; actp, phospho-acetate. The terms bc-acid-CoA and bc-acid refer to the degradation products 2-methylbutanoate, isovalerate, and isobutyrate of the three branched-chain amino acids.

tion of triose phosphates is due to changes in the NADH/NAD$^+$ ratio that affect the activity of glyceraldehyde-3-phosphate dehydrogenase (EC 1.2.1.12), a key regulatory enzyme in the glycolytic pathway of *L. lactis*.

Besides the NADH/NAD$^+$ ratio, the ATP level is shown to have crucial effects on metabolic flux distributions. In *E. faecalis*, changes in the ATP levels are sensed by HPr-kinase/phosphatase (*hprK*, EF1749), a kinase that phosphorylates or dephosphorylates the phosphocarrier protein (HPr; *ptsH*, EF0709) at Ser-46 (P-Ser-HPr), a component of the phosphoenolpyruvate-carbohydrate phosphotransferase system, depending on the intracellular ATP level (57). A complex of P-Ser-HPr and the transcriptional regulatory protein CcpA (*ccpA*, EF1741) were reported to increase the expression of *lldh1* (29, 30). A kinetic inhibition of the PFL in combination with increased *lldh* expression might therefore explain high L-lactate production rates at high glucose concentrations.

Metabolic regulation via global transcription regulators like CcpA-dependent carbon catabolite repression or transcription regulators of the Rex family are common principles in many Gram-positive bacteria. Recent studies on the intracellular human pathogen bacterium *L. monocytogenes* indicate a direct link between metabolism and the expression of virulence genes upon changes in metabolite levels (9). Lobel et al. (9) could link the expression of virulence genes to the global metabolic transcription regulator CodY that responds to changes in the levels of branched-chain amino acids, especially L-isoleucine. It might be interesting to see whether a similar situation is observed for *E. faecalis* and other pathogenic lactic acid bacteria. The levels of L-isoleucine are comparatively low in human blood and might therefore be able to trigger virulence gene expression in these pathogens upon growth in human blood plasma (58).

The incorporation of gene-regulatory information into genome-scale metabolic models might provide novel and valuable insights into metabolic regulation. In combination with the gene-protein-reaction associations integrated here, as well as the consideration of environmental conditions mimicking the human body, this might allow the identification and analysis of essential

genes, proteins, or reactions and the prediction of potential new drug targets.

REFERENCES

1. **Devriese LA, Baele M, Butaye P.** 2006. The genus enterococcus: taxonomy. Prokaryotes **4:**163–147.
2. **Murray BE.** 1990. The life and times of the enterococcus. Clin Microbiol Rev **3:**46–65.
3. **Chavali AK, D'Auria KM, Hewlett EL, Pearson RD, Papin JA.** 2012. A metabolic network approach for the identification and prioritization of antimicrobial drug targets. Trends Microbiol **20:**113–123. http://dx.doi.org/10.1016/j.tim.2011.12.004.
4. **McConville M.** 2014. Open questions: microbes, metabolism and host-pathogen interactions. BMC Biol **12:**18. http://dx.doi.org/10.1186/1741-7007-12-18.
5. **Terzer M, Maynard ND, Covert MW, Stelling J.** 2009. Genome-scale metabolic networks. Wiley Interdisciplinary Rev Syst Biol Med **1:**285–297. http://dx.doi.org/10.1002/wsbm.37.
6. **Price ND, Papin JA, Schilling CH, Palsson BO.** 2003. Genome-scale microbial in silico models: the constraints-based approach. Trends Biotechnol **21:**162–169. http://dx.doi.org/10.1016/S0167-7799(03)00030-1.
7. **Teusink B, Wiersma A, Molenaar D, Francke C, De Vos WM, Siezen RJ, Smid EJ.** 2006. Analysis of growth of *Lactobacillus plantarum* WCFS1 on a complex medium using a genome-scale metabolic model. J Biol Chem **281:**40041–40048. http://dx.doi.org/10.1074/jbc.M606263200.
8. **Flahaut NAL, Wiersma A, Bunt BVD, Martens DE, Schaap PJ, Sijtsma L, Martins dos Santos VA, de Vos WM.** 2013. Genome-scale metabolic model for *Lactococcus lactis* MG1363 and its application to the analysis of flavor formation. Appl Microbiol Biotechnol **97:**8729–8739. http://dx.doi.org/10.1007/s00253-013-5140-2.
9. **Lobel L, Sigal N, Borovok I, Ruppin E, Herskovits AA.** 2012. Integrative genomic analysis identifies isoleucine and CodY as regulators of *Listeria monocytogenes* virulence. PLoS Genet **8:**e1002887. http://dx.doi.org/10.1371/journal.pgen.1002887.
10. **Raman K, Rajagopalan P, Chandra N.** 2005. Flux balance analysis of mycolic acid pathway: targets for anti-tubercular drugs. PLoS Comput Biol **1:**e46. http://dx.doi.org/10.1371/journal.pcbi.0010046.
11. **Raman K, Yeturu K, Chandra N.** 2008. targetTB: a target identification pipeline for *Mycobacterium tuberculosis* through an interactome, reactome, and genome-scale structural analysis. BMC Syst Biol **21:**109–130. http://dx.doi.org/10.1186/1752-0509-2-109.
12. **Sahm DF, Kissinger J, Gilmore MS, Murray PR, Mulder R, Solliday J, Clarke B.** 1989. In vitro susceptibility studies of vancomycin-resistant *Enterococcus faecalis*. Antimicrob Agents Chemother **33:**1588–1591. http://dx.doi.org/10.1128/AAC.33.9.1588.
13. **Fiedler T, Bekker M, Jonsson M, Mehmeti I, Pritzschke A, Siemens N, Nes I, Hugenholtz J, Kreikemeyer B.** 2011. Characterization of three lactic acid bacteria and their isogenic *ldh* deletion mutants shows optimization for YATP (cell mass produced per mole of ATP) at their physiological pHs. Appl Environ Microbiol **77:**612–617. http://dx.doi.org/10.1128/AEM.01838-10.
14. **Alexeeva S, Kort BD, Sawers G, Teixeira de Mattos J HKMJ.** 2000. Effects of limited aeration and of the ArcAB system on intermediary pyruvate catabolism in *Escherichia coli*. J Bacteriol **182:**4934–4940. http://dx.doi.org/10.1128/JB.182.17.4934-4940.2000.
15. **Mehmeti I, Jönsson M, Fergestad EM, Mathiesen G, Nes IF, Holo H.** 2011. Transcriptome, proteome, and metabolite analyses of a lactate dehydrogenase-negative mutant of *Enterococcus faecalis* V583. Appl Environ Microbiol **77:**2406–2413. http://dx.doi.org/10.1128/AEM.02485-10.
16. **Moe KM, Porcellato D, Skeie S.** 2013. Metabolism of milk fat globule membrane components by nonstarter lactic acid bacteria isolated from cheese. J Dairy Sci **96:**727–739. http://dx.doi.org/10.3168/jds.2012-5497.
17. **Thurlow LR, Thomas VC, Hancock LE.** 2009. Capsular polysaccharide production in *Enterococcus faecalis* and contribution of CpsF to capsule serospecificity. J Bacteriol **191:**6203–6210. http://dx.doi.org/10.1128/JB.00592-09.
18. **Holo H, Nes IF.** 1995. Transformation of lactococcus by electroporation. Electroporation Protoc Microorg **47:**195–199. http://dx.doi.org/10.1385/0-89603-310-4:195.
19. **Notebaart RA, van Enckevort FHJ, Francke C, Siezen RJ, Teusink B.** 2006. Accelerating the reconstruction of genome-scale metabolic networks. BMC Bioinformatics **7:**296. http://dx.doi.org/10.1186/1471-2105-7-296.
20. **Thiele I, Palsson BØ.** 2010. A protocol for generating a high-quality genome-scale metabolic reconstruction. Nat Protoc **5:**93–121. http://dx.doi.org/10.1038/nprot.2009.203.
21. **Olivier BG, Rohwer JM, Hofmeyr J-HS.** 2005. Modelling cellular systems with PySCeS. Bioinformatics **21:**560–561. http://dx.doi.org/10.1093/bioinformatics/bti046.
22. **Olivier BG, Bergmann FT.** 2013. SBML level 3 flux balance constraints package, version 1, release 1. Computational Modeling in Biology Network (Combine), United Kingdom. http://identifiers.org/combine.specifications/sbml.level-3.version-1.fbc.version-1.release-1.
23. **Degtyarenko K, de Matos P, Ennis M, Hastings J, Zbinden M, McNaught A, Alcántara R, Darsow M, Guedj M, Ashburner M.** 2008. ChEBI: a database and ontology for chemical entities of biological interest. Nucleic Acids Res **36:**D344–D350. http://dx.doi.org/10.1093/nar/gkm791.
24. **Schuster S, Pfeiffer T, Fell DA.** 2008. Is maximization of molar yield in metabolic networks favored by evolution? J Theor Biol **252:**497–504. http://dx.doi.org/10.1016/j.jtbi.2007.12.008.
25. **Teusink B, Wiersma A, Jacobs L, Notebaart RA, Smid EJ.** 2009. Understanding the adaptive growth strategy of *Lactobacillus plantarum* by in silico optimization. PLoS Comput Biol **5:**1–8. http://dx.doi.org/10.1371/journal.pcbi.1000410.
26. **Mahadevan R, Schilling CH.** 2003. The effects of alternate optimal solutions in constraint-based genome-scale metabolic models. Metab Eng **5:**264–276. http://dx.doi.org/10.1016/j.ymben.2003.09.002.
27. Reference deleted.
28. **Paulsen IT, Banerjei L, Myers GSA, Nelson KE, Seshadri R, Read TD, Fouts DE, Eisen JA, Gill SR, Heidelberg JF, Tettelin H, Dodson RJ, Umayam L, Brinkac L, Beanan M, Daugherty S, DeBoy RT, Durkin S, Kolonay J, Madupu R, Nelson W, Vamathevan J, Tran B, Upton J, Hansen T, Shetty J, Khouri H, Utterback T, Radune D, Ketchum KA, Dougherty BA, Fraser CM.** 2003. Role of mobile DNA in the evolution of vancomycin-resistant *Enterococcus faecalis*. Science **299:**2071–2074. http://dx.doi.org/10.1126/science.1080613.
29. **Verouden MPH, Notebaart RA, Westerhuis JA, van der Werf MJ, Teusink B, Smilde AK.** 2009. Multi-way analysis of flux distributions across multiple conditions. J Chemometrics **23:**406–420. http://dx.doi.org/10.1002/cem.1238.
30. **Oh Y-K, Palsson BO, Park SM, Schilling CH, Mahadevan R.** 2007. Genome-scale reconstruction of metabolic network in *Bacillus subtilis* based on high-throughput phenotyping and gene essentiality data. J Biol Chem **282:**28791–28799. http://dx.doi.org/10.1074/jbc.M703759200.
31. **Feist AM, Henry CS, Reed JL, Krummenacker M, Joyce AR, Karp PD, Broadbelt LJ, Hatzimanikatis V, Palsson BØ.** 2007. A genome-scale metabolic reconstruction for *Escherichia coli* K-12 MG1655 that accounts for 1260 ORFs and thermodynamic information. Mol Syst Biol **3:**121.
32. **Mahadevan R, Edwards JS, Doyle FJ.** 2002. Dynamic flux balance analysis of diauxic growth in *Escherichia coli*. Biophys J **83:**1331–1340. http://dx.doi.org/10.1016/S0006-3495(02)73903-9.
33. **Price ND, Reed JL, Palsson BØ.** 2004. Genome-scale models of microbial cells: evaluating the consequences of constraints. Nat Rev Microbiol **2:**886–897. http://dx.doi.org/10.1038/nrmicro1023.
34. **Orth JD, Thiele I, Palsson BØ.** 2010. What is flux balance analysis? Nat Biotechnol **28:**245–248. http://dx.doi.org/10.1038/nbt.1614.
35. **Tempest DW, Neijssel OM.** 1984. The Status of Yatp and maintenance energy as biologically interpretable phenomena. Annu Rev Microbiol **38:**459–486. http://dx.doi.org/10.1146/annurev.mi.38.100184.002331.
36. **Nielsen J, Villadsen J.** 1992. Modeling of microbial kinetics. Chem Eng Sci **47:**4225–4270. http://dx.doi.org/10.1016/0009-2509(92)85104-J.
37. **Mehmeti I, Faergestad EM, Bekker M, Snipen L, Nes IF, Holo H.** 2012. Growth rate-dependent control in *Enterococcus faecalis*: effects on the transcriptome and proteome, and strong regulation of lactate dehydrogenase. Appl Environ Microbiol **78:**170–176. http://dx.doi.org/10.1128/AEM.06604-11.
38. **Murray BE, Singh KV, Ross RP, Heath JD, Dunny GM, Weinstock GM.** 1993. Generation of restriction map of *Enterococcus faecalis* OG1 and in-

vestigation of growth requirements and regions encoding biosynthetic function. J Bacteriol **175:**5216–5223.

39. **Ardö Y.** 2006. Flavour formation by amino acid catabolism. Biotechnol Adv **24:**238–242. http://dx.doi.org/10.1016/j.biotechadv.2005.11.005.

40. **Liu M, Prakash C, Nauta A, Siezen RJ, Francke C.** 2012. Computational analysis of cysteine and methionine metabolism and its regulation in dairy starter and related bacteria. J Bacteriol **194:**3522–3533. http://dx.doi.org/10.1128/JB.06816-11.

41. **Bos LDJ, Sterk PJ, Schultz MJ.** 2013. Volatile metabolites of pathogens: a systematic review. PLoS Pathog **9:**e1003311. http://dx.doi.org/10.1371/journal.ppat.1003311.

42. **Gitton C, Meyrand M, Wang J, Caron C, Trubuil A, Guillot A, Mistou M, Mistou M-Y.** 2005. Proteomic signature of *Lactococcus lactis* NCDO763 cultivated in milk. Appl Environ Microbiol **71:**7152–7163. http://dx.doi.org/10.1128/AEM.71.11.7152-7163.2005.

43. **Jendresen CB, Martinussen J, Kilstrup M.** 2012. The PurR regulon in *Lactococcus lactis*: transcriptional regulation of the purine nucleotide metabolism and translational machinery. Microbiology **158:**2026–2038. http://dx.doi.org/10.1099/mic.0.059576-0.

44. **Ghadimi H, Pecora P.** 1963. Free amino acids of different kinds of milk. Am J Clin Nutr **13:**75–81.

45. **Hemmilä IA, Mäntsälä PI.** 1978. Purification and properties of glutamate synthase and glutamate dehydrogenase from *Bacillus megaterium*. Biochem J **173:**45–52.

46. **Schreier HJ, Bernlohr RW.** 1984. Purification and properties of glutamate synthase from *Bacillus licheniformis*. J Bacteriol **160:**591–599.

47. **Miller RE, Stadtman ER.** 1972. Glutamate synthase from *Escherichia coli*: an iron-sulfide flavoprotein. J Biol Chem **247:**7407–7419.

48. **Matsuoka K, Kimura K.** 1986. Glutamate synthase from *Bacillus subtilis* PCI 219. J Bacteriol **99:**1087–1100.

49. **Larsen R, Kloosterman TG, Kok J, Kuipers OP.** 2006. GlnR-mediated regulation of nitrogen metabolism in *Lactococcus lactis*. J Bacteriol **188:**4978–4982. http://dx.doi.org/10.1128/JB.00025-06.

50. **Fisher SH.** 1999. Regulation of nitrogen metabolism in *Bacillus subtilis*: vive la différence! Mol Microbiol **32:**223–232.

51. **Holden JT, Bunch JM.** 1973. Asparagine transport in *Lactobacillus plantarum* and *Streptococcus faecalis*. Biochim Biophys Acta **307:**640–655. http://dx.doi.org/10.1016/0005-2736(73)90308-8.

52. **Reid KG, Utech NM, Holden JT.** 1970. Control mechanisms and biochemical genetics: multiple transport components for dicarboxylic amino acids in *Streptococcus faecalis*. J Biol Chem **245:**5261–5272.

53. **Ward DE, Ross RP, van der Weijden CC, Snoep JL, Claiborne A.** 1999. Catabolism of branched-chain α-keto acids in *Enterococcus faecalis*: the *bkd* gene cluster, enzymes, and metabolic route. J Bacteriol **181:**5433–5442.

54. **Ward DE, van der Weijden CC, van der Merwe MJ, Westerhoff HV, Claiborne A, Snoep JL.** 2000. Branched-chain α-keto acid catabolism via the gene products of the *bkd* operon in *Enterococcus faecalis*: a new, secreted metabolite serving as a temporary redox sink. J Bacteriol **182:**3239–3246. http://dx.doi.org/10.1128/JB.182.11.3239-3246.2000.

55. **Vesic D, Kristich CJ.** 2013. A Rex Family Transcriptional repressor influences H$_2$O$_2$ accumulation by *Enterococcus faecalis*. J Bacteriol **195:**1815–1824. http://dx.doi.org/10.1128/JB.02135-12.

56. **Garrigues C, Loubiere P, Lindley ND, Cocaign-Bousquet M.** 1997. Control of the shift from homolactic acid to mixed-acid fermentation in Lactococcus *lactis*: predominant role of the NADH/NAD$^+$ ratio. J Bacteriol **179:**5282–5287.

57. **Kravanja M, Engelmann R, Dossonnet V, Blüggel M, Meyer HE, Frank R, Galinier A, Deutscher J, Schnell N, Hengstenberg W.** 1999. The *hprK* gene of *Enterococcus faecalis* encodes a novel bifunctional enzyme: the HPr kinase/phosphatase. Mol Microbiol **31:**59–66. http://dx.doi.org/10.1046/j.1365-2958.1999.01146.x.

58. **Nasset ES, Heald FP, Calloway DH, Margen S, Schneeman P.** 1979. Amino acids in human blood plasma after single meals of meat, oil, sucrose and whiskey. J Nutr **109:**621–630.

59. **Leenhouts K, Buist G, Bolhuis A, ten Berge A, Kiel J, Mierau I, Dabrowska M, Venema G, Kok J.** 1996. A general system for generating unlabeled gene replacements in bacterial chromosomes. Mol Gen Genet **253:**217–224. http://dx.doi.org/10.1007/s004380050315.